DOI: 10.1002/ejic.200900007

Structures, Redox and Spectroscopic Properties of Pd^{II} and Pt^{II} Complexes Containing an Azo Functionality

Sayak Roy,[a] Ingo Hartenbach,[a] and Biprajit Sarkar*[a]

Keywords: Platinum / Palladium / Azo compounds / EPR spectroscopy / Cyclic voltammetry

The complexes $[PdCl_2(pap)]$ (**1**) and $[PtCl_2(pap)]$ (**2**; pap = 2-phenylazopyridine) were synthesized by treating $PdCl_2$ or K_2PtCl_4, respectively, with pap and characterized by ^1H NMR spectroscopy and elemental analysis. Both these complexes, together with the previously reported complex $[(az)Pd(\mu\text{-}Cl)_2\text{-}Pd(az)]$ (**3**; az = azobenzene), were also characterized by X-ray crystallography. The structures of **1**, **2**, and **3** show a slightly elongated N–N azo double bond due to back-donation from the metal centers and a twisting of the uncoordinated part of the ligands with respect to the rest of the molecule. Cyclic voltammetry of **1**, **2**, **3**, and the related complex $[(az)Pt(\mu\text{-}Cl)_2Pt(az)]$ (**4**) shows reduction processes which are reversible for **1** and **2** but irreversible for **3** and **4**. The first reduction of **1** and **2** leads to radical complexes, and EPR spectroscopy shows the spin to be predominantly located on the azo part of the complexes. The radical complex $\mathbf{2}^{\bullet-}$ shows an unprecedented ^{195}Pt hyperfine coupling constant and g anisotropy for such Pt^{II} radical species. The UV/Vis spectroscopy results for all the complexes are also discussed.

Introduction

Complexes of *cis*-dichloroplatinum with nitrogen co-ligands have been studied for a number of reasons. One major incentive continues to be the use of certain of these complexes in tumor therapy.[1] Another important aspect of such complexes is their one-electron-transfer reactivity. Reversible reduction in such complexes is usually ligand-centered and leads to radical-anion intermediates which often show well observable ^{195}Pt hyperfine coupling in their EPR spectra due to sizeable metal–ligand interactions.[2–6] Luminescence in the solid state or in solution is another fascinating field of research related to such platinum complexes. Such luminescence, which usually occurs from metal-to-ligand charge transfer (MLCT) or intraligand $\pi\rightarrow\pi^*$ excited states, has instigated several structure-spectroscopic correlation studies to clarify their behavior.[7,8] In yet another field of research, Pt^{II} complexes have found use as catalysts and catalyst precursors for C–H bond activation.[9–11] Indeed, one of the first studies of C–H bond activation by transition metal complexes was reported for complexes of Pt^{II} and Pd^{II} with azobenzene.[12] In recent years, complexes of *cis*-dichloropalladium(II) have found use as catalysts and pre-catalysts in a variety of organic transformations.[13] Azo ligands, on the other hand, continue to play an important role in coordination chemistry, with metal complexes of such ligands showing fascinating properties such as photoinduced isomerization and switching.[14–17] Although complexes of $PtCl_2$ and $PdCl_2$ have been studied with a variety of nitrogen- containing π-acceptor ligands,[18,19] there are very few reports of such complexes with ligands containing an azo group.[15,16,20] The ligand 2-phenylazopyridine (pap) has often been used in coordination chemistry.[21–23] Azobenzene (az) has been used for C–H bond activation with metal complexes[12,24] and has been shown to be useful for properties such as switching.[17] Herein we report the synthesis of two complexes containing pap, namely $[PdCl_2(pap)]$ (**1**) and $[PtCl_2(pap)]$ (**2**). The crystal structures of these two complexes are discussed together with the structure of the synthetically known, but hitherto crystallographically uncharacterized, complex $[(az)Pd(\mu\text{-}Cl)_2Pd(az)]$ (**3**). The electrochemical properties of these complexes together with that of $[(az)\text{-}Pt(\mu\text{-}Cl)_2Pt(az)]$ (**4**), as well as their EPR and UV/Vis spectroscopic properties, are discussed below.

Synthesis and Structures

The complexes **1** and **2** (Scheme 1) were obtained in a straightforward manner by treating $PdCl_2$ or K_2PtCl_4, respectively, with pap. Complex **2** could also be obtained by treating pap with $PtCl_2(dmso)_2$. This route required a much shorter reaction time than the first route. Both complexes were characterized by ^1H NMR spectroscopy and elemental analysis.

[a] Institut für Anorganische Chemie, Universität Stuttgart, Pfaffenwaldring 55, 70550 Stuttgart, Germany
Fax: +49-711-6856-4165
E-mail: sarkar@iac.uni-stuttgart.de

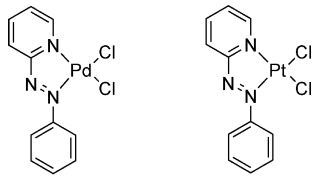

Scheme 1.

Both complexes could be crystallized by slow evaporation of a nitromethane solution at ambient temperature. Complex **1** crystallizes in the *C*2/*c* space group and complex **2** in the *I*2/*a* space group. Crystal data and details of the structure determination are listed in Table 6. Selected bond lengths and angles are given in Tables 1 and 2.

Table 1. Comparison of selected interatomic distances [Å] in one of the three molecules of **1** and **2** and in **3**.

Bond lengths	1	2	3
N1–N2	1.268(16)	1.270(11)	1.289(9)
M–N1	2.017(12)	1.977(9)	2.027(6)
M–N3	2.032(13)	1.946(9)	–
N1–C6	1.449(19)	1.444(11)	–
N2–C5	1.410(18)	1.385(13)	–
M–C1	–	–	1.963(9)
M–Cl	–	–	2.466(2)
N2–C6	–	–	1.389(10)
N1–C7	–	–	1.433(10)

Table 2. Selected bond angles [°] in one of the three molecules of **1** and **2** and in **3**.

Bond angles	1	2	3
N3–M–N1	78.8(5)	77.7(4)	–
N3–M–Cl2	93.8(4)	95.0(3)	–
Cl1–M–Cl2	90.1(2)	89.5(1)	–
N1–M–Cl1	97.5(4)	97.8(3)	–
N1–M–C1	–	–	78.7(3)
C1–M–Cl	–	–	94.7(2)
Cl–M–Cl	–	–	85.3(2)
N1–M–Cl	–	–	101.2(2)
ω	42.2[a]	37.1[a]	40.5[a]

[a] Dihedral angle between the planes of the free phenyl ring and the coordinated part of the ligand.

The metal centers in complexes **1** and **2** (Figures 1 and 2, respectively) adopt an almost square-planar geometry. The N1–M–N3 angles [78.8(5)° for **1** and 77.7(4)° for **2**] are slightly narrower in both complexes than the other angles around the metal centers. This is in keeping with the shorter M–N1 and M–N3 distances compared to the other distances at the metal centers. The N1–N2 azo bond [1.268(16) and 1.270(11) Å for **1** and **2**, respectively] is slightly longer than previously reported N–N double-bonds in azo complexes (1.25 Å).[14,25] This is due to back-donation from the Pd^{II} or Pt^{II} centers into the empty π^* orbital of pap. Such an elongation has previously been observed for other metal complexes containing such azo ligands.[20] In agreement with this back-donation, the N2–C5 distances [1.410(18) and 1.385 Å for **1** and **2**, respectively] are shorter than the N1–C6 distances [1.449(19) and 1.444(11) Å for **1** and **2**, respectively] for both complexes. Averaging out of bond lengths inside a chelate ring after metalation is a typical feature of metal complexes containing azo ligands.[14] The M–N1 and M–N3 distances are almost the same in both **1** and **2**, thereby suggesting equally strong bonding between the metal centers and the pyridine and azo nitrogen atoms. The pyridyl/azo/MCl_2 section of both molecules is essentially planar and adopts a dihedral angle with the phenyl part with values of 42.2° and 37.1° for **1** and **2**, respectively (Figure 3). The phenyl ring twists with respect to the rest of the molecule in order to minimize the steric repulsion between a C–H group of the phenyl ring and the M–Cl bond.[20]

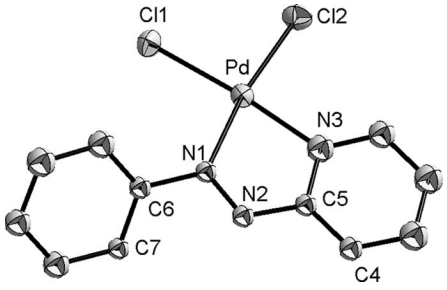

Figure 1. ORTEP view of **1**. The unit cell is constituted of three independent but very similar molecules. Thermal ellipsoids enclose 50% of the electron density.

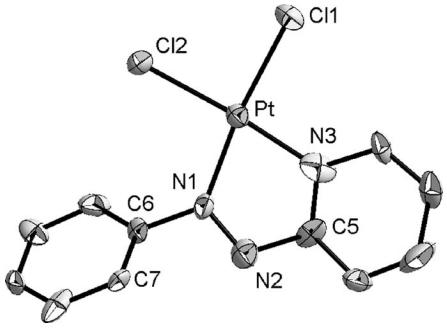

Figure 2. ORTEP view of **2**. The unit cell is constituted of three independent but very similar molecules. Thermal ellipsoids enclose 50% of the electron density.

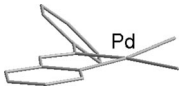

Figure 3. Wireframe view of **1** showing the twisting of the free phenyl part of pap with respect to the rest of the molecule.

Although the synthesis of complex **3** was reported in 1965,[12] and this was the first Pd^{II} complex to show C–H bond activation, to the best of our knowledge there has been no report of its crystal structure to date in the literature. The structures of some related complexes with substituted azobenzenes have, however, been reported.[26] Complex **3** was crystallized by slow diffusion of *n*-hexane into a

dichloromethane solution of the complex at ambient temperature. The complex crystallizes in the $P\bar{1}$ space group. Crystal data and details of the structure determination are listed in Table 6. Selected bond lengths and angles are given in Tables 1 and 2. As in the case of **1** and **2**, the geometry around the Pd^{II} centers in **3** is square planar (Figure 4). The N1–N2 azo bond [1.289(9) Å] is longer than a normal azo N–N double bond[14] due to back-donation from the Pd^{II} center, and this back donation from the metal center means that the N2–C6 bond [1.389(10) Å] is shorter than the N1–C7 bond [1.433(10) Å]. The Pd–Cl′ distance [2.466(2) Å] is longer than the Pd–Cl distance]2.337(2) Å]. This is because of the stronger trans effect exerted by the σ-bonded phenyl ring compared to the nitrogen atom on the azo group.[26] The coordinated phenyl/azo/Pd^{II} parts are essentially planar, with a dihedral angle between this part and the uncoordinated phenyl ring of 40.5°. The twisting of the phenyl ring occurs for the same reasons discussed above for **1** and **2**.

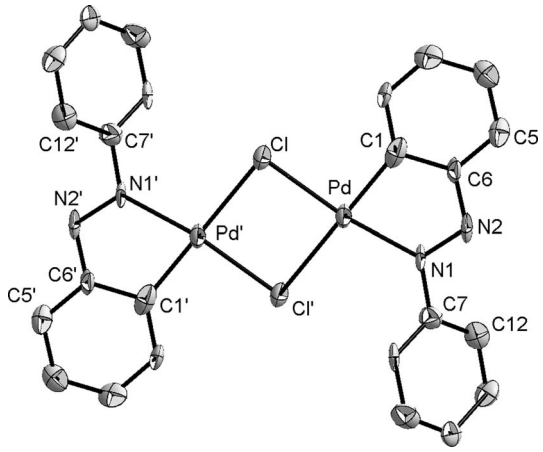

Figure 4. ORTEP view of **3**. Thermal ellipsoids enclose 50% of the electron density.

Cyclic Voltammetry

Complexes **1** and **2** show two well-separated one-electron reduction processes, as can be seen from their cyclic voltammograms in CH_2Cl_2/0.1 M Bu_4NPF_6 (Figure 5). No oxidation processes were observed within the dichloromethane solvent window. Whereas the reduction processes are chemically and electrochemically reversible for **2** at 298 K, complex **1** shows only irreversible reduction processes at that temperature. On cooling to 253 K, however, the first reduction process becomes reversible, although the second reduction of **1** remains irreversible even at lower temperatures. The lability of metal-halide bonds on reduction is much more pronounced for 4d metals than for 5d metals.[27,28] Such lability can sometimes be desirable for certain kinds of catalytic activation.[29,30] The reduction potentials for both complexes are anodically shifted compared to that of the free ligand. Such large anodic shifts illustrate the superb σ-acceptor ability of the $[MCl_2]$ fragments in **1** and **2**.[6] The reduction processes for **1** take place at a less negative potential than those for **2** (–0.59 and –1.39 V for **1** and –0.79 and –1.74 V for **2**). This suggests that the $[PdCl_2]$ fragment has a better σ-acceptor capacity than $[PtCl_2]$ in these complexes. The separation between the two reversible reduction processes in **2** is 0.95 V. This points to a large thermodynamic stability for the one-electron reduced radical complex $\mathbf{2}^{\bullet-}$, as exemplified by the comproportionation constant, K_c, of 10^{16} (Scheme 2). A separation of around 1 V between the two reduction processes is a typical phenomenon for azo complexes.[14] In contrast to **2**, the previously reported complex $[PtCl_2(abpy)]$ (abpy = 2,2′-azobispyridine) shows a complex reduction chemistry, with an irreversible first reduction leading to dimerization of the complex.[20] This difference is probably related to the more robust Pt–Cl bond in **2** and also the lack of a second coordination site in pap as compared to abpy.

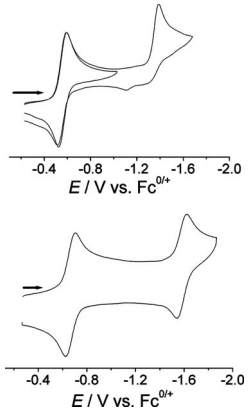

Figure 5. Cyclic voltammogram of **1** (top) at 253 K and **2** (bottom) at 298 K in CH_2Cl_2/0.1 M Bu_4NPF_6. Scan rate: 100 mV/s. Ferrocene/ferrocenium was used as an internal standard.

$$[Pt(pap)Cl_2] \underset{-e^-}{\overset{+e^-}{\rightleftharpoons}} [Pt(pap)Cl_2]^{\bullet-} \underset{-e^-}{\overset{+e^-}{\rightleftharpoons}} [Pt(pap)Cl_2]^{2-}$$

Ox (E_1) Int (E_2) Red

$$\text{comproportionation constant } K_c = \frac{[Int]^2}{[Red][Ox]} = e^{nF\Delta E/RT}$$

Scheme 2.

Complexes **3** and **4** show two irreversible reduction processes, neither of which becomes reversible at either lower temperatures or higher scan rates. Metal-chloride bonds with bridging chlorides are expected to be more labile on reduction than metal-chloride bonds with terminal chlorides, which explains the irreversibility of the reduction processes of **3** and **4** as compared to **1** and **2**. The reduction potentials for **3** are anodically shifted compared to those for **4** (–0.98 V for **3** and –1.38 V for **4** for the first reduction process). This is the same phenomenon as observed for **1** and **2** above. On comparing the reduction potentials of **1** vs. **3** and **2** vs. **4** (Table 3), it can be seen that the complexes with pap are reduced at a less negative potential than the complexes with azobenzene. This can be explained by the fact that pap is a better π-acceptor ligand than az. The dif-

ference between the reduction processes for complexes **3** and **4** is also around 1 V, as expected for complexes with azo ligands (see above). No oxidation processes were observed for either **3** or **4** within the dichloromethane solvent window.

Table 3. Redox potentials of the complexes.[a]

Complex	$E_{1/2}$ (ΔE_p)[b]	$E_{1/2}$ (ΔE_p)[b]
1	–0.56 (65)[c]	–1.39[c,d]
2	–0.79 (70)	–1.74 (80)
3	–0.98[d]	–1.86[d]
4	–1.36[d]	–1.95[d]

[a] Electrochemical potentials in V from cyclic voltammetry in CH_2Cl_2/0.1 M Bu_4NPF_6 at 298 K. Scan rate: 100 mV/s. Ferrocene/ferrocenium was used as internal standard. [b] ΔE_p: difference between peak potentials in mV. [c] Measurements at 253 K. [d] Cathodic peak potential for irreversible reduction.

UV/Vis Spectroscopy

Despite the presence of a low-lying π* orbital, as evidenced by the strongly shifted reduction potentials, particularly for **1** and **2**, the complexes show absorption bands at comparatively higher energies. This can be rationalized by the strong stabilization of the predominantly $[MCl_2]$-centered HOMOs in these complexes. All the complexes show two main features in their absorption spectrum (Figure 6 and Table 4). The long wavelength band (e.g. 512 nm for **2**) is tentatively assigned to a mixture of metal-to-ligand charge transfer (MLCT) with some contribution from halide-to-ligand (XLCT) charge transfer.[6] The next highest energy transition (e.g. 392 for **2**) is most likely a π→π* transition centered on the azo ligands. All the transitions for **1** are shifted to lower energies than for **3**. The same is true on comparing **2** to **4**. This can be justified by invoking the better π-acceptor capability of pap compared to az. On reduction of **2** to $\mathbf{2}^{\bullet-}$, the main bands in the visible region appear at 592 and 480 nm. These can be tentatively assigned to intra-ligand transitions within the pap radical anion and to MLCT transitions. There is very little absorption left in the visible region on further reduction to $\mathbf{2}^{2-}$, as would be expected for a doubly reduced pap ligand bound to $[Pt^{II}Cl_2]$.

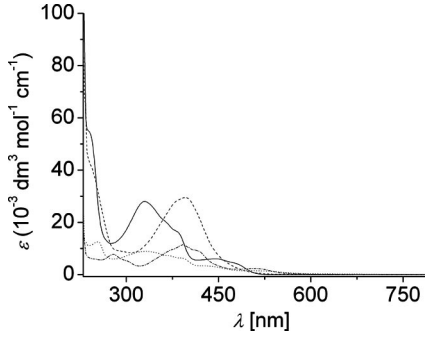

Figure 6. UV/Vis spectra of **1** (---), **2** (-·-·), **3** (−), and **4** (···) in CH_2Cl_2.

Table 4. UV/Vis data for the complexes in CH_2Cl_2.

Complex	λ (ε)[a]
1	243 sh, 397 (29500), 490 (2100)
2	279 (7800), 392 (11400), 415 sh, 512 (2300)
$\mathbf{2}^{\bullet-}$	273 (13100), 302 (13800), 345 sh, 367 (15600), 380 sh, 425 sh, 480 (4100), 592 (1600)
$\mathbf{2}^{2-}$	266 (18200), 290 sh, 355 (10900), 490 sh
3	240 sh, 329 (27900), 382sh, 450 (5900)
4	250 (12600), 330 (9000), 391 sh, 485 sh

[a] Wavelength in nm; molar extinction coefficient in $M^{-1}cm^{-1}$. sh: shoulder.

EPR Spectroscopy

The radical anions $\mathbf{1}^{\bullet-}$ and $\mathbf{2}^{\bullet-}$ can be generated in situ and this has allowed us to study these intermediates in fluid and glassy frozen solutions by EPR spectroscopy. The data obtained from EPR spectroscopic experiments and computer simulations are listed in Table 5 along with data for other related complexes. The dichloroplatinum(II) radical species $\mathbf{2}^{\bullet-}$ (Figure 7) shows a much larger *g* anisotropy and larger ^{195}Pt (I = 1/2) hyperfine coupling than $[PtCl_2(bpy)]^{\bullet-}$[3] and $[PtCl_2(bpym)]^{\bullet-}$, which have very similar values.[6] The azo-based ligand pap has a much lower lying π* orbital than bpy and bpym. The SOMO in the case of $\mathbf{2}^{\bullet-}$ thus has a larger metal contribution as compared to $[Pt(bpy)Cl_2]^{\bullet-}$ and $[Pt(bpym)Cl_2]^{\bullet-}$, which explains the larger Δg and a values for $\mathbf{2}^{\bullet-}$. Despite the large *g* anisotropy and ^{195}Pt hyperfine coupling constant for $\mathbf{2}^{\bullet-}$, which are unprecedented for such radical anions, this radical anion is not a Pt^{I} species. The reduction still predominantly takes place at the azo ligand, with larger metal contributions than in $[PtCl_2(bpy)]^{\bullet-}$ and $[PtCl_2(bpym)]^{\bullet-}$. The a_{Pt} value of 8.5 mT for $\mathbf{2}^{\bullet-}$ represents only a fraction (6.9×10^{-3}) of the isotropic hyperfine coupling constant for platinum (a_0 = 1228 mT).[31] No coupling to the ligand nuclei could be resolved and hence these must have much smaller values than

Table 5. X-band EPR data fo the electrochemically generated first reduced form of the complexes.

	$\mathbf{1}^{\bullet-}$	$\mathbf{2}^{\bullet-}$	$[PtCl_2(bpy)]^{\bullet-}$[a]	$[PtCl_2(bpym)]^{\bullet-}$[a]
g_1[b]	2.007	2.086	2.038	2.034
g_2	2.007	2.007	2.009	2.005
g_3	1.983	1.930	1.935	1.938
Δg[c]	0.024	0.156	0.103	0.096
g_{iso}[d]	2.003	2.002	1.998	1.993
a_1[e]	n.o.	8.5	5.6	5.0
a_2	n.o.	11.2	9.5	6.9
a_3	n.o.	<5.0	–	<3.0
a_{iso}[e]	0.7	8.5	5.4	4.6
Ref.	this work	this work	[3]	[6]

[a] Measurements in dmf. n.o.: not observed. [b] From measurements in glassy frozen solution in CH_2Cl_2/0.1 M Bu_4NPF_6 at 110 K. [c] $\Delta g = g_1 - g_3$. [d] From measurements in CH_2Cl_2/0.1 M Bu_4NPF_6 at 298 K. [e] Metal hyperfine coupling constant in mT as obtained from computer simulation. Line width used for simulating low-temperature spectrum of $\mathbf{2}^{\bullet-}$: 2.2 and 4.5 mT. Lineshape: lorentzian/gaussian, 1/1 (see text for details). For $\mathbf{1}^{\bullet-}$ additionally a_N = 0.9 mT was also determined.

the ^{195}Pt hyperfine coupling constants. The dichloropalladium(II) radical species $\mathbf{1}^{\bullet-}$ has a much smaller *g* anisotropy than $\mathbf{2}^{\bullet-}$. This is the effect of the much smaller spin-orbit coupling constant values of Pd^{II}.[31] The solution EPR spectrum for $\mathbf{1}^{\bullet-}$ (Figure 8) could be simulated well by considering the coupling of the unpaired electron to one Pd nucleus (I = 5/2) with a hyperfine coupling constant of 0.7 mT and an additional coupling to one ^{14}N (I = 1) center with values of 0.9 mT. This is the nitrogen from the azo group which is bound to the Pd center. Even though coupling to the other nitrogen atom of the azo group is expected, this will be smaller than the coupling to the coordinated azo-nitrogen atom. This most likely lies within the linewidth of the spectrum and hence is not resolved.

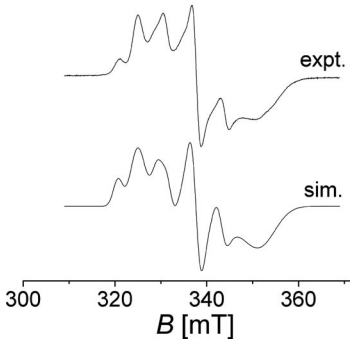

Figure 7. X-band EPR spectrum of electrochemically generated $\mathbf{2}^{\bullet-}$ in CH_2Cl_2/0.1 M Bu_4NPF_6 at 110 K. Frequency: 9.4876 GHz; power: 6.343 mW; modulation amplitude: 0.3 G.

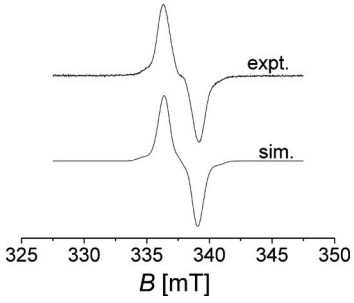

Figure 8. X-band EPR spectrum of electrochemically generated $\mathbf{1}^{\bullet-}$ in CH_2Cl_2/0.1 M Bu_4NPF_6 at 253 K. Frequency: 9.4718 GHz; power: 6.339 mW; modulation amplitude: 0.2 G.

Conclusions

Using the ligand pap we have been able to synthesize and fully characterize the complexes **1** and **2**. The structural data of **1** and **2**, together with that of the previously reported complex **3**, show a slightly elongated N–N azo double bond and twisting of the non-coordinated part of the ligands around the rest of the molecule. Whereas the reduction of **3** and **4** proceeds irreversibly even at lower temperatures, the first reduction of **1** or **2** leads to stable radical intermediates where the spin is predominantly located on the azo part of the complexes. The EPR spectrum of $\mathbf{2}^{\bullet-}$ shows an unusually large ^{195}Pt hyperfine coupling constant and *g* anisotropy in comparison to other related Pt^{II} radical anions. The utility of such complexes, and of related complexes with other azo ligands, in catalytic ethylene poly- and oligomerization is currently under investigation.

Experimental Section

Instrumentation: ^1H NMR spectra were recorded at 250.13 MHz with a Bruker AC250 instrument. EPR spectra in the X band were recorded with a Bruker System EMX connected to an ER 4131 VT variable temperature accessory. EPR simulations were performed using the Simfonia software of Bruker. The EPR spectra were simulated by considering the natural abundance of the various isotopes involved. For EPR measurements, the paramagnetic species were generated directly inside the EPR tube using a two-electrode cell. UV/Vis/NIR absorption spectra were recorded with a Shimadzu UV 3101 PC spectrophotometer. Cyclic voltammetry was carried out in 0.1 M Bu_4NPF_6 solution using a three-electrode configuration (glassy carbon working electrode, Pt counter electrode, Ag wire as pseudo-reference) and a PAR 273 potentiostat and function generator. The ferrocene/ferrocenium (Fc/Fc^+) couple served as internal reference. Elemental analysis was performed with a Perkin–Elmer Analyser 240.

General Considerations: The ligand pap was synthesized under normal atmospheric conditions using reagent-grade solvents. For the metal complexes, all manipulations were carried out using Schlenk techniques under argon. The solvents used for metal complex synthesis were dried and distilled under argon and degassed by common techniques prior to use. Azobenzene was purchased from Sigma–Aldrich. The precursor $PdCl_2$ was purchased from Acros and K_2PtCl_4 from ABCR. The ligand pap and complexes **3** and **4** were synthesized according to literature procedures.[12,22]

Synthesis of $[PdCl_2(pap)]$ (1):[32] A mixture of palladium(II) dichloride (50 mg, 0.28 mmol) and pap (51 mg, 0.28 mmol) was stirred in ethanol for 4 h at room temperature. A bright yellow precipitate formed during this time. This solid was filtered off, washed with methanol, and dried in vacuo. Yield 75 mg (74%) ^1H NMR ($CDCl_3$): δ = 7.51 (m, 2 H), 7.63 (m, 1 H), 7.82 (m, 1 H), 8.01 (d, 2 H), 8.34 (m, 1 H), 8.44 (m, 1 H), 9.35 (d, J = 4 Hz, 1 H) ppm. IR (solid): $\nu_{N=N}$ = 1603 cm^{-1}. $C_{11}H_9Cl_2N_3Pd$ (360.51): calcd. C 36.65, H 2.52, N 11.66; found C 36.35, H 2.55, N 11.51.

Synthesis of $[PtCl_2(pap)]$ (2).[33] **Route A:** A mixture of potassium tetrachloroplatinate (50 mg, 0.12 mmol) and pap (20 mg, 0.12 mmol) was dissolved in a mixture of water and dioxane (1:1) and allowed to stand for 7 d. A dark crystalline solid precipitated. This solid was filtered off, washed two or three times with dioxane and dried in vacuo. Yield 32 mg (60%).

Route B: A mixture of $PtCl_2(dmso)_2$ (174 mg, 0.412 mmol) and pap (75 mg, 0.412 mmol) was heated to reflux in 40 mL of nitromethane for 5 h. The solution turned dark brown during this time. After removal of the solvent, the crude product was recrystallized from a mixture of nitromethane and diethyl ether. The product was finally filtered off and washed with diethyl ether. Yield 102 mg (56%). ^1H NMR ([D_6]acetone): δ = 7.63 (m, 3 H), 7.92 (m, 2 H), 8.30 (m, 1 H), 8.69 (td, J = 7.7, 1.6 Hz, 1 H), 8.83 (m, 1 H) ppm. IR (solid): $\nu_{N=N}$ = 1606 cm^{-1}. $C_{11}H_9Cl_2N_3Pt$ (449.20): calcd. C 29.41, H 2.05, N 9.04; found C 29.49, H 2.05, N 9.04.

Crystal Structure Determination: Single crystals were grown by slow evaporation of a nitromethane solution at ambient temperature (for

1 and **2**) or by layering a dichloromethane solution of the complex with *n*-hexane at ambient temperature (for **3**). A suitable crystal was selected under a layer of viscous hydrocarbon oil, attached to a glass fiber, and instantly placed in a low-temperature N_2 stream. The selected single crystals were measured using Mo-K_α radiation (λ = 0.71073 Å) at 173 K. Calculations were performed with the SHELXTL PC 5.03 and SHELXL-97[34,35] program system installed on a local PC. The structures were solved by direct methods and refined on F_o^2 by full-matrix least-squares refinement. Anisotropic thermal parameters were included for all non-hydrogen atoms. Further details can be found in Table 6. CCDC-714302 (for **1**), -714303 (for **2**), and -714301 (for **3**) contain the supplementary crystallographic data for this paper. These data can be obtained free of charge from the Cambridge Crystallographic Data Centre via www.ccdc.cam.uk/data_request.cif.

Table 6. Crystal data and details of the structure determination for complexes **1**–**3**.

	1	**2**	**3**
Empirical formula	$C_{11}H_9Cl_2N_3Pd$	$C_{11}H_9Cl_2N_3Pt$	$C_{24}H_{18}Cl_2N_4Pd_2$
a [Å]	55.460(3)	14.1202(5)	3.9515(3)
b [Å]	9.3386(7)	9.3784(4)	10.9806(8)
c [Å]	13.9813(11)	55.0598(16)	12.9995(11)
α [°]	90	90	71.546(5)
β [°]	98.733(5)	95.444(3)	89.888(5)
γ [°]	90	90	84.149(5)
Cell volume [Å^3]	7157.2(9)	7258.4(5)	531.98(7)
ρ(calcd.) [g cm^{-3}]	2.007	2.466	2.017
M_r [g mol^{-1}]	360.51	449.20	646.14
Z	8	8	2
Crystal system	monoclinic	monoclinic	triclinic
Space group	*C*2/*c*	*I*2/*a*	$P\bar{1}$
T [K]	100(1)	150(2)	100(1)
Radiation, λ [pm]	71.073	71.073	71.073
Abs. coeff. [cm^{-1}]	1.981	12.018	1.963
Reflections	11690	29152	4682
Unique reflections, R_{int}	4713, 0.087	16171, 0.1433	2560, 0.0933
Parameters	248	463	145
R values	R_1 = 0.0763 wR_2 = 0.1441	R_1 = 0.0735 wR_2 = 0.1275	R_1 = 0.0661 wR_2 = 0.1384
Goodness of fit	1.128	0.948	1.044
Largest electron density difference/hole [e Å^{-3}]	1.101/–1.027	4.06/–2.32	1.934/–2.147

Acknowledgments

B. S. is indebted to the Landesstiftung Baden-Württemberg for the financial support of this research project through the Elite Programme for Postdocs. Ralph Huebner is kindly acknowledged for carrying out the UV/Vis spectroelectrochemical measurements.

[1] B. Lippert, *Cisplatin*, Wiley-VCH, Weinheim, Germany, **1999**.
[2] S. A. MacGregor, E. J. L. McInnes, R. J. Sorbie, L. J. Yellowlees, in: *Molecular Electrochemistry of Inorganic Bioinorganic and Organometallic Compounds* (Eds.: A. J. L. Pombeiro, A. J. McCleverty), Kluwer Academic Publishers, Dordrecht, The Netherlands, **1993**, p. 503.
[3] D. Collison, E. J. L. McInnes, F. E. Mabbs, K. J. Taylor, A. J. Welch, L. J. Yellowlees, *J. Chem. Soc., Dalton Trans.* **1996**, 329.
[4] E. J. L. McInnes, R. D. Farley, S. A. Macgregor, K. J. Taylor, L. J. Yellowlees, C. C. Rowlands, *J. Chem. Soc. Faraday Trans.* **1998**, *94*, 2985.
[5] E. J. L. McInnes, R. D. Farley, C. C. Rowlands, A. Welch, L. Rovatti, L. J. Yellowlees, *J. Chem. Soc., Dalton Trans.* **1999**, 4203.
[6] W. Kaim, A. Dogan, M. Wanner, A. Klein, I. Tiritiris, T. Schleid, D. J. Stufkens, T. L. Scoeck, E. J. L. McInnes, J. Fiedler, S. Zalis, *Inorg. Chem.* **2002**, *41*, 4139.
[7] W. B. Connick, V. M. Miskowski, V. H. Houlding, H. B. Gray, *Inorg. Chem.* **2000**, *39*, 2585.
[8] K. E. Dungey, B. D. Thompson, N. A. P. Ken-Maguire, L. L. Wright, *Inorg. Chem.* **2000**, *39*, 5192.
[9] L. Johansson, M. Tilset, *J. Am. Chem. Soc.* **2001**, *123*, 739.
[10] R. A. Periana, D. J. Taube, S. Gamble, H. Taube, T. Satoh, H. Fujii, *Science* **1998**, *280*, 560.
[11] X. Fang, B. L. Scott, J. G. Watkin, G. J. Kubas, *Organometallics* **2000**, *19*, 4193.
[12] A. C. Cope, R. W. Siekman, *J. Am. Chem. Soc.* **1965**, *87*, 3272.
[13] P. Braunstein, *J. Organomet. Chem.* **2004**, *689*, 3953.
[14] W. Kaim, *Coord. Chem. Rev.* **2001**, *219–221*, 463.
[15] H. Kirsch, P. Holzmeier, *Adv. Organomet. Chem.* **1992**, *34*, 67.
[16] T. Yukuta, I. Mori, M. Kurihara, J. Mizutani, N. Tamai, T. Kawai, M. Irie, H. Nishihara, *Inorg. Chem.* **2002**, *41*, 7143.
[17] S. Kume, H. Nishihara, *Dalton Trans.* **2008**, 3260.
[18] P. S. Braterman, J.-I. Song, C. Vogler, W. Kaim, *Inorg. Chem.* **1992**, *31*, 222.
[19] A. Klein, J. v. Slageren, S. Zalis, *Eur. J. Inorg. Chem.* **2003**, 1917.
[20] A. Dogan, B. Sarkar, A. Klein, F. Lissner, T. Schleid, J. Fiedler, S. Zalis, V. K. Jain, W. Kaim, *Inorg. Chem.* **2004**, *43*, 5973.
[21] B. K. Santra, G. A. Thakur, P. Ghosh, A. Pramanik, G. K. Lahiri, *Inorg. Chem.* **1996**, *35*, 3050.
[22] G. K. Lahiri, S. Bhattacharya, S. Goswami, A. Chakravorty, *J. Chem. Soc., Dalton Trans.* **1990**, 561.
[23] S. Patra, B. Sarkar, S. Maji, J. Fiedler, F. A. Urbanos, R. J.-Aparicio, W. Kaim, G. K. Lahiri, *Chem. Eur. J.* **2006**, *12*, 489.
[24] D. Babic, M. Curic, K. Molcanov, G. Ilc, J. Plavec, *Inorg. Chem.* **2008**, *47*, 10446.
[25] B. Sarkar, S. Patra, J. Fiedler, R. B. Sunoj, D. Janardanan, G. K. Lahiri, W. Kaim, *J. Am. Chem. Soc.* **2008**, *130*, 3532.
[26] S. Armentano, A. Crispini, G. d. Munno, M. Ghedini, F. Neve, *Acta Crystallogr., Sect. C* **1991**, *47*, 966.
[27] S. Frantz, R. Reinhardt, S. Greulich, M. Wanner, J. Fiedler, C. Duboc-Toia, W. Kaim, *Dalton Trans.* **2003**, 3370.
[28] A. K. Das, E. Bulak, B. Sarkar, F. Lissner, T. Schleid, M. Niemeyer, J. Fiedler, W. Kaim, *Organometallics* **2008**, *27*, 218.
[29] U. Koelle, M. Graetzel, *Angew. Chem. Int. Ed. Engl.* **1987**, *26*, 568.
[30] S. Chardon-Noblat, S. Cosnier, A. Deronzier, N. Vlachopoulus, *J. Electroanal. Chem.* **1993**, *352*, 213.
[31] J. A. Weil, J. R. Bolton, *Electron Paramagnetic Resonance*, 2nd ed., John Wiley & Sons, New Jersey, **2007**.
[32] C. K. Pal, S. Chattopadhyay, C. Sinha, D. Bandyopadhyay, A. Chakravorty, *Polyhedron* **1994**, *13*, 999.
[33] G. K. Rauth, S. Pal, D. Das, C. Sinha, A. M. Z. Slawin, J. D. Woollins, *Polyhedron* **2001**, *20*, 363.
[34] G. M. Sheldrick, *Program for crystal structure solution and refinement*, University of Göttingen, Germany, **1997**.
[35] W. Herrendorf, H. Bärnighausen, *Program HABITUS*, Karlsruhe, Germany, **1993**.

Received: January 4, 2009
Published Online: April 8, 2009

